Spectroscopy of the binary TNO Mors–Somnus with the JWST and its relationship to the cold classical and plutino subpopulations observed in the DiSCo-TNO project

A. Souza-Feliciano, B. Holler, N. Pinilla-Alonso, M. de Prá, R. Brunetto, T. Müller, J. Stansberry, J. Licandro, J. Emery, E. Henault, et al.

A&A, 681, L17 (2024)
https://doi.org/10.1051/0004-6361/202348222

Astronomy & Astrophysics

LETTER TO THE EDITOR

Spectroscopy of the binary TNO Mors–Somnus with the JWST and its relationship to the cold classical and plutino subpopulations observed in the DiSCo-TNO project

A. C. Souza-Feliciano[1], B. J. Holler[2], N. Pinilla-Alonso[1], M. De Prá[1], R. Brunetto[3], T. Müller[4], J. Stansberry[2,5,6], J. Licandro[7,8], J. P. Emery[5], E. Henault[3], A. Guilbert-Lepoutre[9], Y. Pendleton[10], D. Cruikshank[10], C. Schambeau[1], M. Bannister[11], N. Peixinho[12], L. McClure[5], B. Harvison[1,10], and V. Lorenzi[7,13]

[1] Florida Space Institute, University of Central Florida, Orlando, FL, USA
e-mail: astro.carol@ucf.edu
[2] Space Telescope Science Institute, Baltimore, MD, USA
[3] Université Paris-Saclay, CNRS, Institut d'Astrophysique Spatiale, Orsay, France
[4] Max-Planck-Institut für extraterrestrische Physik, Garching, Germany
[5] Northern Arizona University, Flagstaff, AZ, USA
[6] Lowell Observatory, Flagstaff, AZ, USA
[7] Instituto de Astrofisica de Canarias, La Laguna, Tenerife, Spain
[8] Universidad de La Laguna, Departamento de Astrofisica, La Laguna, Tenerife, Spain
[9] Laboratoire de Géologie de Lyon: Terre, Planètes, Environnement, UMR 5276 CNRS, UCBL, ENSL, Villeurbanne, France
[10] University of Central Florida, Department of Physics, Orlando, FL, USA
[11] University of Canterbury, School of Physical and Chemical Sciences – Te Kura Matū, Christchurch, New Zealand
[12] Instituto de Astrofísica e Ciências do Espaço, Departamento de Física, Universidade de Coimbra, Coimbra, Portugal
[13] Fundación Galileo Galilei-INAF, Tenerife, Spain

Received 10 October 2023 / Accepted 9 January 2023

ABSTRACT

Context. Trans-Neptunian objects (TNOs) are remnants of small icy bodies from planetary formation that orbit in the region beyond Neptune. Within the population of TNOs, Trans-Neptunian binaries (TNBs) provide a valuable opportunity to test the models of the formation and evolution of planetesimals in the trans-Neptunian region. Various theories have been proposed to describe the observed separations between binary components, their relative sizes, and other orbital parameters. The colors of TNOs have been used to trace the dynamical history of the outer Solar System and the colors of TNB components provide tests for formation theories. However, spectral information for the components of small TNBs, crucial information that could validate formation mechanisms, has until now remained elusive.

Aims. The main goal of this work is to characterize the near-infrared spectral properties of the TNB plutino (341520) Mors–Somnus, the only TNB with resolved components in the *James Webb* Space Telescope (JWST) Large Cycle 1 General Observer program "DiSCo-TNOs" (PID 2418; PI: Pinilla-Alonso). The secondary goal is to use the surface compositions of the individual components of the Mors–Somnus system to probe formation and dynamical evolution in the outer Solar System through comparison to the surface properties of the cold classical and plutino (3:2 resonant) dynamical groups.

Methods. To achieve these goals, we measured the spectral slope of the continuum and identified absorption bands in the individual spectra of Mors and Somnus, as well as in those of the cold classicals and plutinos obtained with the NIRSpec Integral Field Unit (IFU) and the PRISM/CLEAR disperser (0.6–5.3 μm), and compared these results to shed light on the dynamical evolution of the Mors–Somnus binary.

Results. The spectra of Mors and Somnus are similar and indicate the presence of complex organic materials, CO_2, CO, OH-compounds, and tentative nitrogen-rich materials. We find a high degree of compositional diversity in the plutino population, a group of TNOs that likely formed elsewhere and moved to their current orbits during the migration of Neptune, while the cold classical TNOs, which likely formed in situ, appear more homogeneous.

Conclusions. The very wide separation between the components, their nearly equal sizes, and the high orbital inclination of the system suggest this plutino binary is a survivor of the primordial population of objects beyond 30 au. The similarities found between the spectral features of the plutinos Mors and Somnus and those of all of the cold classical TNOs in the DiSCo-TNOs sample as well as the high degree of compositional heterogeneity found in the plutino population provide compositional evidence for evaluation of Neptune's migration in the trans-Neptunian region early on in the history of the Solar System.

Key words. methods: observational – techniques: spectroscopic – Kuiper belt: general – Kuiper belt objects: individual: (341520) Mors–Somnus

1. Introduction

Trans-Neptunian objects (TNOs) are remnants of small icy bodies from planetary formation occupying orbits in the region beyond Neptune. By studying their dynamical, physical, and compositional properties, we can obtain clues as to the chemical and physical conditions of the early Solar System. Due to their sizes, which range from tens of kilometers (e.g., (486958) Arrokoth) to TNOs smaller than the dwarf planets ($D \lesssim 1000$ km), they are expected to retain pristine materials that were present in the protoplanetary disk, which include numerous ices and refractory compounds (e.g., Barucci & Merlin 2020; Pinilla-Alonso et al. 2023; McClure et al. 2023). The dynamical structure of the trans-Neptunian region contains the footprint of planetary migration that took place during approximately the first gigayear of the history of the Solar System (e.g., Levison et al. 2008; Nesvorný et al. 2010). Trans-Neptunian binaries (TNBs), in addition to carrying all this information, are an essential tracer of TNO formation and evolutionary mechanisms. Characterization of the secondary orbit allows the determination of the system mass and, for systems with a known effective diameter, their bulk density. The separation, relative sizes, and system density, combined with other orbital and physical parameters, have provided the means for the development of various formation scenarios, and the colors of TNBs have been used to gain valuable insights into the evolutionary history of TNOs and a first-degree approximation to surface composition.

TNB formation models can be broadly divided into two categories: those explaining large primaries with relatively small satellites on relatively tight orbits (with respect to the primary radius), such as Pluto-Charon, (136199) Eris-Dysnomia, and (50000) Quaoar-Weywot; and those explaining small, comparably sized objects with relatively wide separations, such as the binary systems discussed in Parker et al. (2011). The first category is more compatible with formation through collisions (e.g., Stern 2002; Brown et al. 2006; Canup 2010; Grundy et al. 2019), while the streaming instability scenario provides a reasonable explanation for the second category of comparably sized components with wide separations, similar colors (Youdin & Goodman 2005; Jacquet et al. 2011), and prograde orbits (Nesvorný & Vokrouhlický 2019). Nesvorný et al. (2010) showed that the formation of a binary is the natural outcome of the gravitational collapse of a cloud of pebbles with significant angular momentum in the streaming instability scenario. Their simulations of gravitational collapse showed that the typical semi-major axes, eccentricities, and size ratios of the observed binaries are well reproduced by that model. It is worth noting that this process is also thought to be responsible for the formation of contact binaries, which are systems composed of comparably sized components on extremely tight orbits, such that the two components are in contact, as in the case of (486958) Arrokoth. Following the formation of a wider binary in the streaming instability scenario, dynamical friction or gas drag would result in evolution onto a tighter orbit (McKinnon et al. 2020). The similarity in colors between the two components (Benecchi et al. 2009) is a natural consequence of the fact that they are made of the same material. The TNB (341520) Mors–Somnus (provisional designation 2004 TY430, hereafter, Mors–Somnus) could have formed through the streaming instability mechanism, because the sizes of its components, the mutual semi-major axis, its colors, and its prograde orbit are all in agreement with the model (Benecchi et al. 2009; Nesvorný et al. 2010).

Mors–Somnus belongs to the group of objects trapped in the 3:2 resonance with Neptune (Sheppard et al. 2012). Pluto is also trapped in the same resonance, resulting in the name "plutinos" for this subpopulation of resonant TNOs. Mors–Somnus belongs to the category of equal-size binaries[1], with the primary (Mors) and secondary (Somnus) having computed diameters of <116 km and <110 km (Thirouin et al. 2014), respectively, and a separation of $21\,000 \pm 160$ km (Sheppard et al. 2012; Thirouin et al. 2014). Due to their equal size, ultra-red visible spectral slope (36 ± 2 %/1000 Å; Sheppard et al. 2012), and very wide relative separation ($a/R_{\rm primary} \approx 180$), Mors–Somnus was initially considered to be a dynamically cold classical TNO that was transported to the 3:2 resonance early on in Solar System history (Sheppard et al. 2012; Thirouin & Sheppard 2018). However, Nesvorný & Vokrouhlický (2019) analyzed the binary survival rate in the outer Solar System and a very wide, fragile binary such as Mors–Somnus would not survive this process. In order to survive, the widely separated TNB would have had to start beyond the reach of Neptune at >30 au, with ~37–39 au being the most plausible formation distance for Mors–Somnus (Nesvorný 2015), and be transported to the 3:2 mean-motion resonance with Neptune by gentler mechanisms (Hahn & Malhotra 2005). The comparison of the spectral properties of Mors–Somnus with the cold classical TNOs, which are well known for having formed beyond 30 au ($42 < a < 47$ au), and plutinos, which had 99% of their population captured from the massive primordial disk inside of 30 au (Nesvorný 2015), can add a surface compositional element to the dynamical history of this binary.

The "Discovering the composition of the trans-Neptunian objects, icy embryos for planet formation" (DiSCo-TNOs) project (PID: 2418, PI: Pinilla-Alonso) is the Large Cycle 1 General Observer (GO) program of the *James Webb* Space Telescope (JWST) focusing on near-infrared spectroscopy of TNOs. The program observed 59 TNOs and Centaurs, including 12 TNBs. Of the 12 binary pairs observed in this program, Mors–Somnus is the only one that is spatially resolved; the fluxes of each component of the other TNBs are blended. In regard to the dynamical classes, the DiSCo-TNOs project observed five cold classical TNOs ((79360) Sila-Numan, (523591) 2001 QD298, (469705) Kágára, (385437) 2003 GH55, and (66652) Borasisi) and six plutinos ((38628) Huya, (444745) 2007 JF43, (120216) 2004 EW95, (47171) Lempo, (455502) 2003 UZ413, and (612533) 2002 XV93). Here we present the spectra in the wavelength range of 0.7–5.1 μm of the two components of the binary Mors–Somnus, which is resolved as two separated point sources accompanied by the spectra of five cold classical TNOs and six plutinos for the purposes of comparison. We discuss the implications of the surface compositions of Mors and Somnus for the origins of the binary and the dynamical evolution of the outer Solar System based on comparisons of the two objects with one another and of the binary with the larger TNO population.

2. Observations

The spectra of Mors–Somnus were obtained on January 22, 2023 (UT), during observation 45 of PID 2418. The NIRSpec Integral Field Unit (IFU), using the PRISM/CLEAR spectral element, was employed for the observation. This configuration allowed the acquisition of low-resolution spectra ($R \sim 30$–300) across a $3'' \times 3''$ field of view over a wavelength range of 0.6–5.3 μm

[1] $R_2/R_1 > 0.5$, where R_1 and R_2 are the radii of primary and secondary components, respectively (Noll et al. 2020).

Table 1. Observational circumstances and physical properties of the sample.

Object	Mid-obs. time (UT)	ET (s)	V (mag)	Δ (au)	r (au)	α (°)	Class	D (km) [(*)]	p_V
(341520) Mors–Somnus	2023-01-22 13:05:12	2451	21.65	28.65	29.05	1.80	P	116/110	<0.12
(79360) Sila-Nunam	2022-11-22 16:37:29	2451	21.84	43.37	43.42	1.31	CC	343 [(*)]	0.09
(385437) 2003 GH55	2023-07-22 15:13:30	2568	22.34	40.75	41.28	1.23	CC	178	0.15
(523591) 2001 QD298	2023-06-12 16:17:09	2684	22.65	42.12	42.14	1.39	CC	233	0.07
(469705) Kágára	2023-05-08 20:28:04	2684	22.36	39.60	40.22	1.39	CC	174 [(*)]	0.16
(66652) Borasisi	2022-11-05 05:34:43	2684	22.27	41.78	42.48	1.16	CC	163 [(*)]	0.24
(444745) 2007 JF43	2023-03-05 23:26:52	1459	21.24	36.48	36.5	1.57	P	–	–
(38628) Huya	2023-03-13 12:55:29	759	19.65	28.91	28.95	1.98	P	458 [(*)]	0.08
(47171) Lempo	2023-01-22 11:15:31	820	20.03	30.53	30.84	1.76	P	393 [(*)]	0.08
(612533) 2002 XV93	2022-11-03 13:42:36	1225	20.85	37.64	38.13	1.32	P	549	0.04
(120216) 2004 EW95	2023-02-22 01:32:48	1225	20.83	27.16	27.16	2.21	P	291	0.04
(455502) 2003 UZ413	2023-02-14 05:31:20	1404	21.00	44.62	44.70	1.27	P	670	0.07

Notes. "Mid-obs. time (UT)" refers to the mid-observation time; "ET (s)" is the total exposure time in seconds for each object; "V (mag)" is the visual magnitude at the time of the observation; "Class" is the dynamical classification, with P = plutino and CC = cold classical; D is the diameter; and p_V is the visible geometric albedo. Albedos and diameters for Mors–Somnus are from Thirouin et al. (2014) and from the "TNOs are Cool" database (Müller et al. 2020) for the other TNOs. [(*)]For TNBs in our sample, the diameter shown is for the combined system.

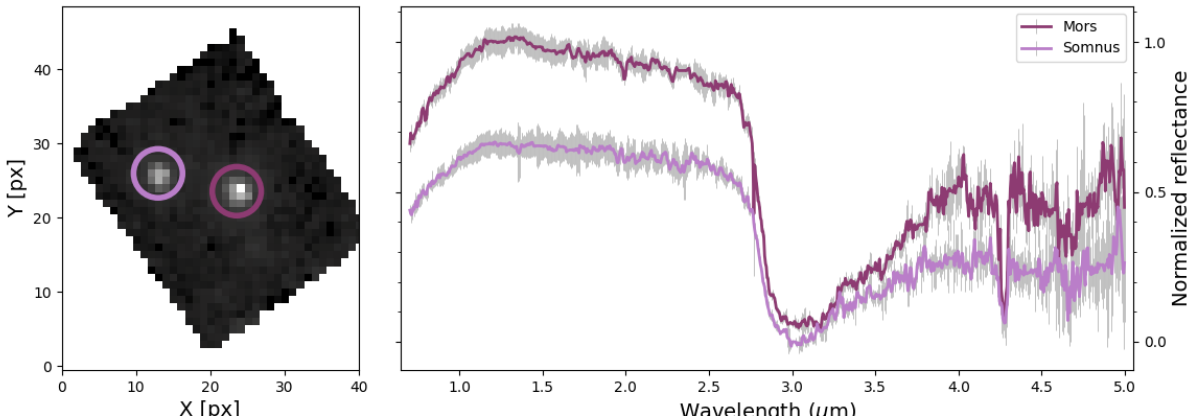

Fig. 1. Spectral data cube and near-infrared spectra of Mors–Somnus. Left: A single slice of the spectral data cube obtained by the NIRSpec IFU showing the resolved Mors (primary – dark purple circle) and Somnus (secondary – light purple circle) TNO binary system. The separation between the two components is ∼1100 mas. Right: Normalized reflectance of Mors at 1.25 μm (dark purple line) and Somnus reflectance scaled to Mors (light purple line) after removal of the solar contribution versus wavelength (μm). The 1σ uncertainties are represented by the light gray bars.

(Böker et al. 2022). (This wavelength range was trimmed to 0.7–5.1 μm to remove noisier edge regions; see Appendix A.) At the time of the observation (Table 1), the two components of the binary were separated by 1100 mas, which could be resolved with the 100 mas plate scale of the IFU (Fig. 1, left side). The observing sequence started at 12:44:30 UT on January 22, 2023, and finished on the same day at 13:34:50 UT. We obtained four dithers of 613 s each. Accounting for overheads and pointing, these observations required 6867 s[2]. Details of the observational circumstances of Mors–Somnus, the cold classical TNOs, and plutinos can be found in Table 1.

The step-by-step data-reduction process and spectral extraction can be found in Appendix A. For all objects in our sample, we combined the fluxes of the four dithers and divided this by the combined flux of the star SNAP-2 (G3V type; Gordon et al. 2022) (Fig. A.1), which was also observed with the NIRSpec/IFU and the PRISM/CLEAR spectral element (PID 1128, PI: Lutzgendorf). The normalized reflectance spectrum of each component of Mors and Somnus, displaying the relative difference in fluxes between the sources, can be seen in Fig. 1 (right side). The normalized spectra of Mors and Somnus are shown in Fig. 2, while the spectra for the cold classical TNOs and plutinos can be seen in Fig. 3.

3. Analysis and results

3.1. Mors and Somnus

Here we present the first spectra obtained for the plutinos Mors and Somnus (Fig. 1, right panel). As can be seen, both spectra show similar spectral behavior across the observed wavelength range, with Mors presenting 1.5 times the flux of Somnus at 1.21 μm, corresponding to a difference of 0.44 mag between the components at this wavelength. Sheppard et al. (2012) and Sheppard & Trujillo (2008) found a maximum difference of 0.3 mag between this pair and a mean difference of 0.1 mag.

In the normalized spectra (Fig. 2, top), we measured the spectral slope of each spectrum in two separate ranges, both

[2] For more details, consult the APT file at https://www.stsci.edu/jwst/science-execution/program-information?id=2418

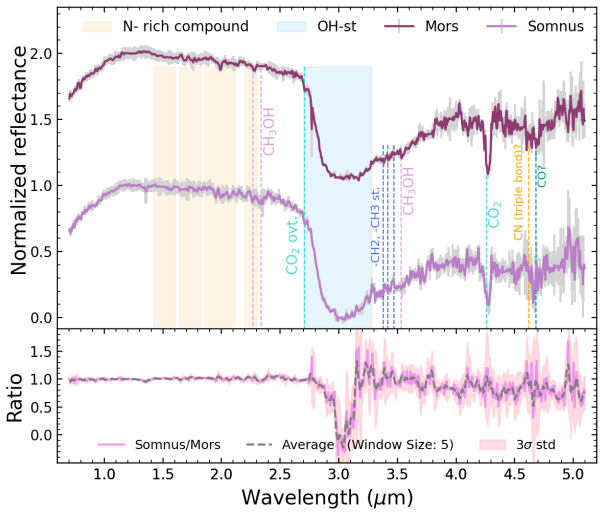

Fig. 2. Ice species identification in the spectra of Mors and Somnus. Top: Tentative species identifications in the spectra of Mors (dark purple) and Somnus (light purple). The spectra were both normalized at 1.25 μm and the spectrum of Mors was shifted 1.0 units up for clarity. The dashed vertical lines represent the center positions of the molecular absorption features. The shaded regions represent where the listed materials can absorb. Methanol (CH_3OH) is shown in pink, carbon dioxide (CO_2) and its overtones in light green, carbon monoxide (CO) in teal, OH-stretch in light blue, carbon-nitrogen-rich compounds in orange, and aliphatic complex organic molecules in dark blue. The gray bars represent the 1σ errors associated with the normalized spectra. Bottom: Ratio between the spectrum of Somnus and Mors (pink line). The average moving ratio is shown as a gray dashed line (window size = 5), and the 3σ standard deviation is shown as a pink shaded region.

in units of %/1000 Å: from 0.65 to 1.2 μm (SIR'_1) and from 1.15 to 2.25 μm (SIR'_2), normalizing at 1.175 μm. These values are similar for each target – within the uncertainties – with $SIR'_1 > SIR'_2$ and $SIR'_2 < 0$ for both targets (Table 2). This provides a first hint that both components of the binary system share a similar composition. The ratio of Mors and Somnus spectra is shown in Fig. 2 (bottom) and the spectra are similar at the 3σ level. The main difference appears in the range between 3 and 3.2 microns, which could be attributed to invalid values on Somnus' dither 1 (Fig. A.1) in this wavelength range, or to the very low flux in this region. For these possible reasons, we do not attribute a physical meaning to this difference.

The spectral similarity is strengthened by the fact that the main features present in Mors' spectrum also exist in Somnus' (Fig. 2, top). Both spectra show a deep absorption band around 3 μm caused by the OH-stretching mode; this could be associated with any molecule with an OH-bond (blue vertical region). At 4.26 μm, we see the fundamental carbon dioxide (CO_2) absorption band (light green vertical dashed line) and, at 2.7 μm, its overtone. The indication of complex organic molecules by the red visible spectral slope is confirmed in both targets by the aliphatic organic features between 3.3 and 3.6 μm (dashed blue lines; Raponi et al. 2020). As a tentative detection, we see an absorption band between 4.55 and 4.75 μm that could be indicative of carbon monoxide, which shows its fundamental band at 4.68 μm, and C≡N (triple bond) at 4.60 μm (Cruikshank et al. 1991). The C≡N bond has several overtones at 1.75 μm, 2 μm, and 2.3 μm that cannot be confidently detected in Mors and Somnus. Another material that could be attributed to the features at 2.27 μm in Mors and 2.27 and 2.34 μm in Somnus is methanol ice (pink vertical dashed lines), which has two combination bands at those wavelengths (Cruikshank et al. 1998) and its fundamental at 3.53 μm; although this latter cannot be totally resolved due to the other complex organic bands around 3.3 and 3.6 μm. The features at 2.27 and 2.34 μm associated with methanol have been seen in other TNOs, such as (486958) Arrokoth (Grundy et al. 2020), (55638) 2002 VE95 (Merlin et al. 2012), and (5145) Pholus (Cruikshank et al. 1998). Besides those features, the decrease in signal-to-noise ratio for $\lambda > 4.5$ μm prevents us from confidently assigning the other structures seen in both spectra. Overall, both components exhibit strikingly similar surface compositions, with no clear detection of water ice in their top surface layers, indications of CH- and N-bearing species that could have been accreted during the early stages of their formation, and by-products of the irradiation of lighter C-bearing molecules in coexistence with CO_2, CO, and CH_3OH.

3.2. Cold classical and "plutino" TNOs

For the purposes of comparison to Mors and Somnus, we present the spectra of the cold classical TNOs (79360) Sila-Numan, (523591) 2001 QD298, (469705) Kágára, (385437) 2003 GH55, and (66652) Borasisi, and for the plutinos (38628) Huya, (444745) 2007 JF43, (120216) 2004 EW95, (47171) Lempo, (455502) 2003 UZ413, and (612533) 2002 XV93 from 0.7 to 5.1 μm. Until now no spectra have been reported in the literature for 2001 QD298, Kágára, 2003 GH55, 2007 JF43, and 2002 XV93 in any wavelength range. Despite Sila-Nunam, Borasisi, Huya, and Lempo being binary or multiple systems, they were not resolved by the NIRSpec/IFU observations. Instead, we are presenting unresolved spectra of these multiple systems.

The spectra of all the cold classical TNOs in our sample (blue colored group of spectra in Fig. 3) have similar red SIR'_1 and neutral/bluish SIR'_2 spectral slopes to those found for Mors and Somnus, taking into account the errors associated with the measurements (Table 2). The cold classical TNOs also show spectral structures similar to those presented in the Mors and Somnus spectra (see Fig. 3 and Table 2). Previous studies suggested CH_4 on the surface of Borasisi (Dalle Ore et al. 2015), but we do not identify any absorption features that could be associated with CH_4 in its near-infrared spectrum.

In the plutino class (brown-orange colored group of spectra in Fig. 3), the spectra of 2007 JF43, Lempo, and Huya share some similarities to Mors–Somnus and the cold classical TNOs, presenting the aforementioned features. For Huya, methanol ice was predicted by Souza-Feliciano et al. (2018). In the case of 2007 JF43, the bands associated with the C≡N compound are deeper than in the other objects. The other three plutinos in our sample have different spectral shapes. The objects 2004 EW95, 2003 UY413, and 2002 XV93 have clear indications of crystalline water ice. Both amorphous and crystalline water ice present bands centered at 1.5, 2.0, 3.0, and 4.5 μm. However, the reflectance peak at 3.1 microns corresponds only to the Fresnel peak of crystalline water ice. Amorphous water ice does not present unique features in this wavelength region, and so detailed modeling is required to confirm its presence. However, amorphization of crystalline water ice via cosmic-ray irradiation is a relatively fast process (e.g., Cooper et al. 2003; Cook et al. 2007), and typical temperatures in the trans-Neptunian region (~40 K) imply an equilibrium between these two phases (e.g., Zheng et al. 2009; Holler et al. 2017). Therefore, the clear identification of crystalline water ice in the spectra of these objects provides strong indirect evidence for the presence of amorphous water ice. These objects have higher SIR'_2 spectral slopes than

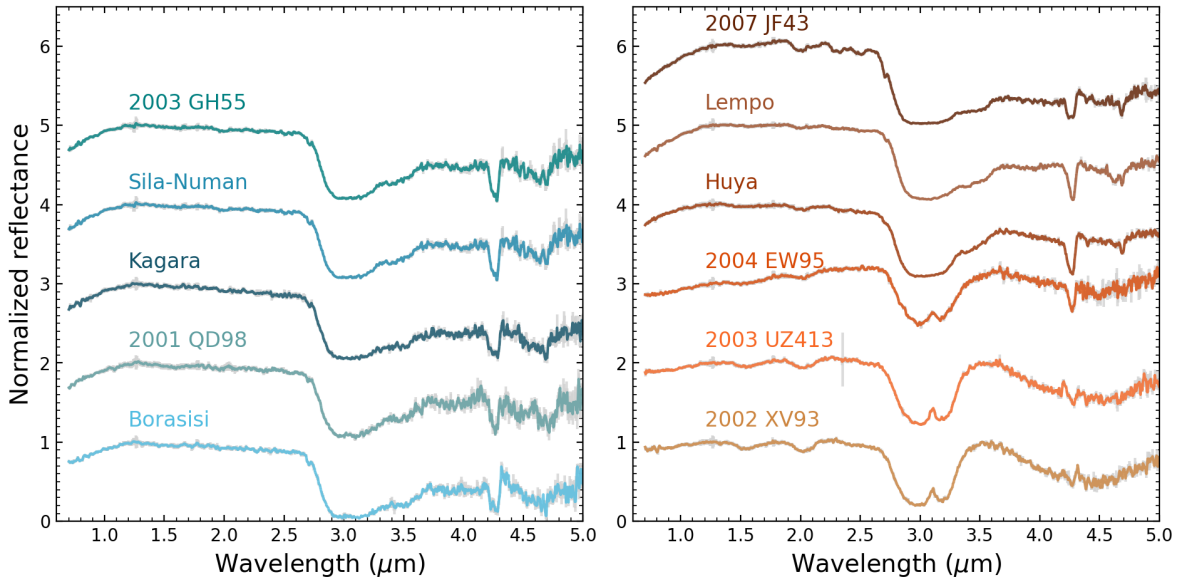

Fig. 3. Cold classical and plutino populations in the DiSCo-TNOs sample. Reflectance spectra of cold-classical objects (left panel, blue shades) and plutinos (right panel, brown-orange shades) in the DiSCo-TNOs sample. All spectra were normalized at 1.25 μm and vertically shifted for clarity. The light gray bars represent the 1σ errors associated with the normalized spectra.

Mors, Somnus, and the cold classical TNOs, and shallower CO_2 absorption bands (see Fig. 3). Concerning the spectrum from 0.4 to 0.9 μm of 2004 EW95 (Seccull et al. 2018), which shows features that were attributed to phyllosilicates and are comparable to the features seen in the spectra of hydrated C-type asteroids, the spectrum from 0.7 to 5.1 μm of 2004 EW95 presented here, does not confirm the presence of these materials. Phyllosilicates show signatures at 2.7 and 3.1 μm (Rivkin et al. 2002; Hamilton et al. 2019) that are not present on the 2004 EW95 spectrum; instead, it shows clear signatures of water ice in crystalline and amorphous phases, and carbon dioxide, similarly to two other two TNOs (2002 XV93 and 2003 UY413) in our sample. In general, the cold classical TNOs in our sample resemble each other and the plutinos show a higher degree of variety regarding their surface compositions.

4. Discussion

The remarkable resemblance in the surface compositions of Mors and Somnus suggests that they formed together in the outer part of the protoplanetary disk. This result endorses dynamical theories of same-size binary formation in the trans-Neptunian region, and specifically the streaming instability scenario (Nesvorný et al. 2010; Nesvorný 2015; Nesvorný & Vokrouhlický 2019). The difference in the reflectance level for Mors and Somnus (see Fig. 1, right side) according to their size and albedo estimations (Table 1) should be around 1.1, and we see a difference of ∼1.5 on their relative reflectances, translating to a maximum difference in magnitude of 0.44 mag, while the maximum reported was 0.3 mag (Sheppard et al. 2012). As both objects share a similar surface composition (see Sect. 3), it is improbable that the entire difference relies on a difference in albedo between the two components. The sizes and albedos of these targets were obtained by lower bounds estimated through rotational light-curve measurements (Thirouin et al. 2014). New size measurements are necessary to properly interpret the difference in relative reflectance between these targets.

Table 2. Spectral slopes of Mors and Somnus (first block), cold classical TNOs (second block), and plutinos (third block) from the DiSCo-TNOs sample.

Object	SIR'_1 (%/1000 Å)	SIR'_2 (%/1000 Å)
Mors	6.71 ± 0.22	–0.83 ± 0.11
Somnus	7.06 ± 0.22	–0.61 ± 0.13
2003 GH55	7.42 ± 0.14	–0.65 ± 0.05
Sila-Nunam	6.35 ± 0.16	–0.70 ± 0.05
Kágára	6.05 ± 0.22	–0.99 ± 0.08
2001 QD298	5.83 ± 0.17	–0.81 ± 0.06
Borasisi	5.42 ± 0.14	–0.87 ± 0.05
2007 JF43	8.88 ± 0.16	–0.30 ± 0.05
Lempo	7.50 ± 0.13	–0.28 ± 0.04
Huya	4.84 ± 0.17	–0.54 ± 0.05
2004 EW95	2.98 ± 0.16	1.73 ± 0.05
2003 UZ413	2.37 ± 0.16	0.50 ± 0.06
2002 XV93	1.97 ± 0.17	0.04 ± 0.05

Notes. SIR'_1 is measured from 0.65 to 1.2 μm and SIR'_2 from 1.15 to 2.25 μm. See Sect. 3 for calculation details.

When compared to the other TNOs in our sample, Mors and Somnus share spectral similarities with all the cold classical TNOs. The cold classical TNOs are thought to orbit in the region where they were formed, remaining undisturbed during Neptune's migration (Parker & Kavelaars 2010). As a consequence, the degree of compositional diversity in the cold classical TNOs should be low when compared with other dynamical populations. All the spectra of the cold classical TNOs in our sample have similar structures in terms of slopes and molecular detections. In this respect, our compositional analysis provides observational constraints to the formation models of this population.

On the other hand, the degree of diversity among the six plutinos presented in our sample is worth mentioning. Three of

them (2004 EW95, 2003 UY413, and 2002 XV93) show strong absorption bands due to crystalline and amorphous water ice phases, while 2007 JF43 and Lempo do not. The spectra of 2007 JF43, Lempo, and Huya are also compatible with the spectra of Mors, Somnus, and the cold classical TNOs. All of these elements reinforce the theoretical scenario for the formation of the 3:2 mean-motion resonance with Neptune, with objects implanted there from several regions in the outer protoplanetary disk (e.g., Nesvorný 2015).

5. Conclusions

We present the first resolved spectra (0.7–5.1 μm) of the small, widely separated plutino binary Mors–Somnus, which were obtained as part of the DiSCo-TNOs project using JWST's NIRSpec IFU. The surface compositions of Mors and Somnus are similar, supporting the streaming instability formation scenario for binaries of similar size and wide separation (Nesvorný et al. 2010; Nesvorný 2015; Nesvorný & Vokrouhlický 2019). Their spectral features from 0.7 to 5.1 μm support a surface composition compatible with complex organic materials, C- and N-rich compounds, CO_2, CO, and some indications of CH_3OH. Additionally, we show the spectra of five cold classical TNOs (Sila-Numan, 2001 QD298, Kágára, 2003 GH55, and Borasisi) and six plutinos (Huya, 2007 JF43, 2004 EW95, Lempo, 2003 UZ413, and 2002 XV93). We find a high degree of compositional diversity in the plutino population, a group of TNOs that likely formed elsewhere and moved to their current orbits during the migration of Neptune, while the cold classical TNOs, which likely formed in situ, appear more homogeneous. By comparing the surface composition of Mors and Somnus with both dynamical groups, we find an increased level of compatibility with the cold classical TNOs than with the plutinos, suggesting that the Mors–Somnus binary formed at a heliocentric distance >30 au, similar to the cold classical population. In addition to the properties of this binary being more closely related to those of the cold classical TNOs, we provide compositional evidence of the effects of Neptune's migration in the sculpting of the trans-Neptunian region.

Acknowledgements. This work is based on observations made with the NASA/ESA/CSA *James Webb* Space Telescope as part of the GO1 programs #2418 (support for this program was provided by NASA through a grant from the Space Telescope Science Institute) and #1128. The data were obtained from the Mikulski Archive for Space Telescopes at the Space Telescope Science Institute, which is operated by the Association of Universities for Research in Astronomy, Inc., under NASA contract NAS 5-03127 for JWST. The DiSCo-TNOs team would like to thank Weston Eck and Alaina Henry of STScI for their help in preparing the observations for execution. N.P. acknowledges funding by Fundação para a Ciência e a Tecnologia (FCT) through the research grants UIDB/04434/2020 and UIDP/04434/2020. J.A.S. acknowledges generous sabbatical support by Northern Arizona University and by the Lowell Observatory visiting astronomer program. R.B. and E.H. acknowledge support from the CNES-France (JWST mission). A.G.L. has received funding from the European Research Council (ERC) under the European Union's Horizon 2020 research and innovation program (Grant Agreement No. 802699).

References

Barucci, M. A., & Merlin, F. 2020, in The Trans-Neptunian Solar System, eds. D. Prialnik, M. A. Barucci, & L. Young (Elsevier), 109
Benecchi, S., Noll, K., Grundy, W., et al. 2009, Icarus, 200, 292
Böker, T., Arribas, S., Lützgendorf, N., et al. 2022, A&A, 661, A82
Brown, M. E., Van Dam, M., Bouchez, A., et al. 2006, ApJ, 639, L43
Canup, R. M. 2010, AJ, 141, 35
Cook, J. C., Desch, S. J., Roush, T. L., Trujillo, C. A., & Geballe, T. R. 2007, ApJ, 663, 1406
Cooper, J. F., Christian, E. R., Richardson, J. D., & Wang, C. 2003, Earth Moon Planets, 92, 261
Cruikshank, D. P., Allamandola, L. J., Hartmann, W. K., et al. 1991, Icarus, 94, 345
Cruikshank, D., Roush, T., Bartholomew, M., et al. 1998, Icarus, 135, 389
Dalle Ore, C. M., Barucci, M., Emery, J., et al. 2015, Icarus, 252, 311
Gordon, K. D., Bohlin, R., Sloan, G. C., et al. 2022, AJ, 163, 267
Grundy, W., Noll, K., Roe, H., et al. 2019, Icarus, 334, 62
Grundy, W. M., Bird, M. K., Britt, D. T., et al. 2020, Science, 367, aay3705
Hahn, J. M., & Malhotra, R. 2005, AJ, 130, 2392
Hamilton, V. E., Simon, A. A., Christensen, P. R., et al. 2019, Nat. Astron., 3, 332
Holler, B. J., Young, L. A., Buie, M. W., et al. 2017, Icarus, 284, 394
Jacquet, E., Balbus, S., & Latter, H. 2011, MNRAS, 415, 3591
Levison, H. F., Morbidelli, A., VanLaerhoven, C., Gomes, R., & Tsiganis, K. 2008, Icarus, 196, 258
McClure, M. K., Rocha, W. R. M., Pontoppidan, K. M., et al. 2023, Nat. Astron., 7, 431
McKinnon, W. B., Richardson, D. C., Marohnic, J. C., et al. 2020, Science, 367, aay6620
Merlin, F., Quirico, E., Barucci, M., & De Bergh, C. 2012, A&A, 544, A20
Müller, T., Lellouch, E., & Fornasier, S. 2020, in The Trans-Neptunian Solar System, eds. D. Prialnik, M. A. Barucci, & L. Young, 153
Nesvorný, D. 2015, AJ, 150, 68
Nesvorný, D., & Vokrouhlický, D. 2019, Icarus, 331, 49
Nesvorný, D., Youdin, A. N., & Richardson, D. C. 2010, AJ, 140, 785
Noll, K. S., Grundy, W. M., Nesvorný, D., & Thirouin, A. 2020, The Trans-Neptunian Solar System (Elsevier), 205
Parker, A. H., & Kavelaars, J. 2010, ApJ, 722, L204
Parker, A. H., Kavelaars, J., Petit, J.-M., et al. 2011, ApJ, 743, 1
Pinilla-Alonso, N., de Prá, M., & Souza-Feliciano, A. C. 2023, Planetary Systems Now (World Scientific), 305
Raponi, A., Ciarniello, M., Capaccioni, F., et al. 2020, Nat. Astron., 4, 500
Rivkin, A. S., Howell, E. S., Vilas, F., & Lebofsky, L. A. 2002, Asteroids III (Tucson: University of Arizona Press), 235
Seccull, T., Fraser, W. C., Puzia, T. H., Brown, M. E., & Schönebeck, F. 2018, ApJ, 855, L26
Sheppard, S. S., & Trujillo, C. A. 2008, IAU Circ., 8962, 2
Sheppard, S. S., Ragozzine, D., & Trujillo, C. 2012, AJ, 143, 58
Souza-Feliciano, A. C., Alvarez-Candal, A., & Jiménez-Teja, Y. 2018, A&A, 614, A92
Stern, S. A. 2002, AJ, 124, 2300
Thirouin, A., & Sheppard, S. S. 2018, AJ, 155, 248
Thirouin, A., Noll, K. S., Ortiz, J. L., & Morales, N. 2014, A&A, 569, A3
Youdin, A. N., & Goodman, J. 2005, ApJ, 620, 459
Zheng, W., Jewitt, D., & Kaiser, R. I. 2009, J. Phys. Chem. A, 113, 11174

Appendix A: Data reduction

To ensure the most up-to-date calibration, the *uncal* data for each observation were downloaded from the Barbara A. Mikulski Archive for Space Telescopes (MAST) using the *jwst_mast_query* tool and locally run through the latest version of the JWST data calibration pipeline. All data presented in this paper were processed using pipeline v1.11.4 and context file *jwst_1119.pmap*. The pipeline was run with all default parameters but with an added "destriping" step to remove the $1/f$ pattern noise. First, the Detector1 and Spec2 steps of the pipeline were run, with the *cal* file output from Spec2 used to construct a mask with all NaN values set to 1 and all non-NaN values set to NaN. The *rate* file output by the Detector1 step was then multiplied by the mask to mask out the illuminated portions of the detector. Additionally, the central ∼200 rows of the *rate* file were masked out due to leakage through the NIRSpec fixed slits. A ±200-pixel moving median was calculated along each column for each pixel in that column, with the result subtracted from that pixel in the original, unmasked *rate* file. The Spec2 step was then rerun on the destriped *rate* file, producing a calibrated spectral data cube (an *s3d* file) for each dither.

The spectral extraction step made use of a "template PSF-fitting" routine. The procedure described below was applied to each component of the binary separately, while the flux of the other component was masked. For single sources, no additional mask was necessary. We first constructed the wavelength array using the CRVAL3 and CDELT3 header keywords. The DQ (data quality) extension in the fits files was then used to identify pixels flagged by the pipeline; any pixel with a value of >0 was set to NaN for the remainder of the extraction. The rough centroid position was determined by eye and the remaining outlier pixels (due to artifacts or background objects) more than 5 pixels from the centroid position were set to NaN. The background was then calculated in each slice using the median of all pixels >5 pixels from the centroid and subtracted from the slice. Stepping through the spectral data cube one slice at a time, a template PSF was calculated as the median of the ten background-subtracted slices ahead of and behind the slice under consideration (inclusive), for a total of 21 slices. The template PSF was trimmed to a 9×9 vignette to reduce the leverage of distant pixels in the fit, with all pixels outside the box set to NaN, and normalized to unity within the vignette. The template PSF was then iteratively fit to the slice under consideration (with the background included), using the ratio of the template PSF to the data and the median background as initial guesses for the fitting routine. The *scipy.optimize.minimize* function was used with a Nelder-Mead (amoeba) method to determine the best-fit values for the flux scaling factor and the background. After each of the three iterations, the model (template PSF times flux scaling factor plus the background) was subtracted from the data and all pixels >5-σ from the mean were considered outliers and set to NaN. The final PSF model was calculated by multiplying each slice of the template PSF by the flux scaling factor, and the flux was extracted from the template PSF model within a 3.5-pixel-radius circular aperture centered on the PSF centroid. The same extraction method was used for the standard star SNAP-2 in program 1128 (PI: Lutzgendorf).

Fluxes extracted from individual dithers were then combined and a solar-flux correction was performed. All dithers for the standard star were resampled onto the same wavelength grid and a median was computed within each wavelength bin. Three iterations of outlier rejection were then performed: a 21-point moving median and standard deviation were calculated and any points >3-σ were replaced with the median value. For Mors-Somnus, the extracted spectra from all dithers were resampled onto the same wavelength grid as the standard star, and a median was performed, followed by a division of the median by the standard star. Outlier rejection was then performed on the corrected Mors and Somnus spectra. Uncertainties on each median spectrum were computed as the median absolute deviation within each wavelength bin, and uncertainties were propagated for the solar-corrected spectra.

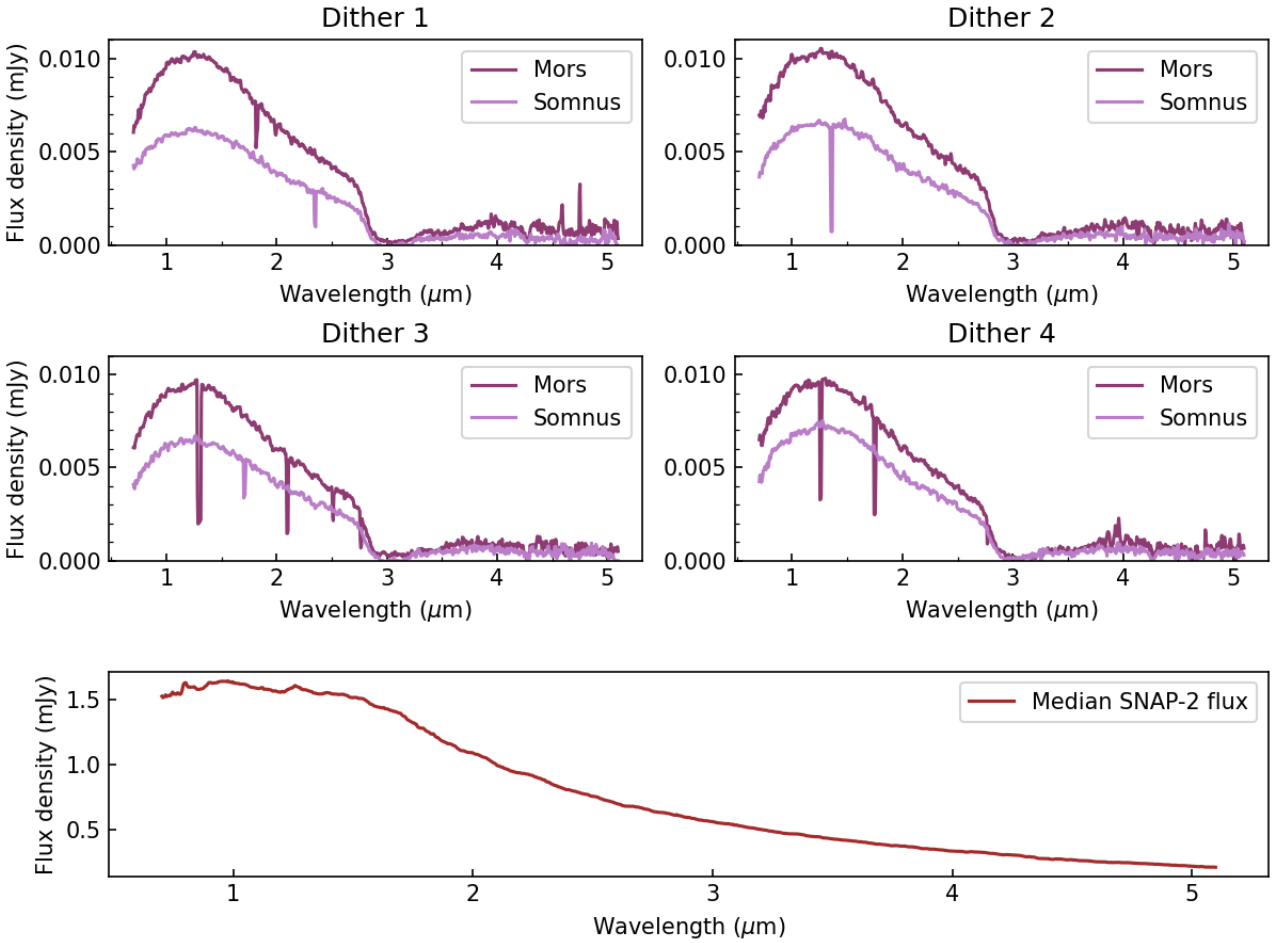

Fig. A.1. Extracted flux density (y-axis) in mJy for each dither of Mors (dark purple line) and Somnus (light purple line) versus wavelength (x-axis in μm). The spectrum of the G3V-type star SNAP-2 used to correct the TNO spectra for the reflected solar component is shown in the bottom panel of the figure.